# Hysteresis and the single-phase metal-insulator transition in switchable $YH_x$ films

E. S. Kooij, A. T. M. van Gogh, D. G. Nagengast, N. J. Koeman, and R. Griessen
*Faculty of Sciences, Division of Physics and Astronomy, Vrije Universiteit, De Boelelaan 1081, 1081 HV Amsterdam, The Netherlands*
(Received 21 March 2000)

Extraordinary large hysteresis effects in optical, electrical, and structural properties are observed in switchable mirrors based on thin yttrium hydride ($YH_x$) films, deposited on quartz glass or sapphire. The pressure-composition isotherms of the $YH_x$ system between $x=2$ and 3 for absorption and desorption, determined electrochemically, differ by approximately three orders of magnitude. The optical transmittance exhibits a distinct minimum when loading the films from the dihydride to the trihydride state; however, upon unloading this minimum is absent. The desorption data are in good agreement with literature data on bulk yttrium, but the absorption results show large deviations. Most important for the metal-insulator transition is that during hydrogen loading $YH_x$ remains in a single hcp phase for $x>2.1$. The hysteresis is discussed in terms of strains (and consequently stress) at the interface between fcc dihydride and hcp trihydride.

## I. INTRODUCTION

Owing to their application for efficient hydrogen storage and in rechargeable batteries, metal-hydrogen ($MH_x$) systems have been the subject of extensive research over the past century.[1,2] Thermodynamics, crystallography, transport properties, magnetism, electronic band structure, and superconductivity have been investigated in great detail in many $MH_x$ systems. As most of these studies were done on bulk material, the optical characterization of metal hydrides was limited to absorbance and reflectance spectroscopy.[3,4]

The use of thin-film techniques in the preparation of $MH_x$ samples introduced exciting possibilities for investigating these materials, and as a result many intriguing phenomena were observed. For example, it has been shown for palladium that the reduced film thickness has a marked effect on the thermodynamic phase diagram; for thin films the critical temperature appears to be lowered considerably, indicating a weakening of the elastic H-H interaction energy.[5,6]

The discovery of switchable mirrors based on rare earth metal hydrides ($RH_x$) was another result of the use of thin films in the study of $MH_x$ systems. Huiberts *et al.*[7] showed that hydrogen absorption in yttrium and lanthanum induces a metal-insulator transition accompanied by drastic optical changes; the initially reflecting metal transforms into a transparent insulator. Since this report, several authors have described similar optical switching properties in other $RH_x$ and in alloys based on these materials.[8–15]

Hydrogenation of switchable mirrors can be achieved either by exposing the sample to a hydrogen gas atmosphere,[7–10] electrochemically by polarization in a suitable electrolyte solution,[14–17] or chemically by immersion in a $NaBH_4$ solution.[18] The major advantage of electrochemical loading is the ability to control the hydrogen concentration. Under oxygen-free conditions the hydrogenation reaction

$$Y + xH_2O + xe^- \rightleftarrows YH_x + xOH^- \qquad (1)$$

implies that the change of the hydrogen concentration $\Delta x$ is proportional to the transferred charge (or equivalently, the current integrated over time). Additionally, the electrochemical potential is related to an effective hydrogen gas pressure, thereby offering the possibility to study the thermodynamic properties of the system.

In our study of the physics of switchable yttrium films we have encountered extremely large hysteresis effects upon varying the hydrogen concentration. Under normal conditions (room temperature, atmospheric pressure) the hydrogen concentration $x$ in yttrium hydride ($YH_x$) can be varied reversibly between $\beta$-$YH_{2+\delta}$ and $\gamma$-$YH_{3-\delta}$, both in electrochemical and gas-phase experiments. Lower concentrations can only be reached by desorption at considerably higher temperatures ($\sim 1000$ K).[19] To our knowledge this is the first report of such large hysteresis, either in bulk material or thin films of any metal hydride.

In this paper we describe the influence of this hysteresis on various physical quantities measured during hydrogen absorption and desorption in the reversible concentration range ($1.9 \leqslant x < 3.0$). Optical transmittance and reflectance, pressure-composition isotherms, and resistivity are measured *in situ* during electrochemical hydrogenation. The crystallographic structure is determined by x-ray diffraction in a gas-phase loading experiment, and related to the electrolytic experiments by means of the simultaneously measured resistivity. The desorption and absorption characteristics of the $YH_x$ system are discussed separately. We show that the desorption data correspond quite well to what has been reported for bulk material, while the absorption results show that a hexagonal single phase exists already for $x \gtrsim 2.1$ in $YH_x$. Finally, the hysteretic behavior, resulting from the difference in loading and unloading, is discussed in terms of stress and strain at the interface between cubic dihydride and hexagonal trihydride.

## II. EXPERIMENT

Yttrium films of 300-nm thickness are evaporated in an ultrahigh vacuum (UHV) system (pressure $10^{-9}$ mbar during evaporation) on quartz (Suprasil 1, Heraeus) disks of 40-mm diameter. To prevent yttrium from oxidation, and to catalyze hydrogenation, a cap layer of 15-nm palladium is deposited *in situ*. After removing them from the UHV sys-

 

tem, the samples are contacted using conducting adhesive (E-Solder 3021, EPOXY Produkte GmbH). Subsequently, the contacts are shielded from the electrolyte using an insulating lacquer (Apiezon). In all experiments an initial hydrogen concentration $x=0.08$ H/Y is taken into account.[20]

Electrochemical experiments are performed using an EG&G Princeton Applied Research (PAR) 263A Potentiostat/Galvanostat in a three-electrode configuration. A platinum sheet is used as a counterelectrode in a separate compartment connected by a glass frit to the compartment containing the working and reference electrodes. The glass frit is used to hinder diffusion of $O_2$, evolved at the counterelectrode, through the electrolyte to the working electrode. The yttrium/palladium sample is used as the working electrode. A Hg/HgO electrode in 1-M KOH is used as a reference. All potentials are given with respect to this reference electrode.

For single-wavelength transmittance measurements a diode laser (Melles Griot, $\lambda=635$ nm) is used. The transmitted intensity is measured with a standard photodiode in combination with a linear current-to-voltage amplifier. Spectrally resolved transmittance and reflectance measurements are performed by placing the electrochemical cell in a Bruker IFS 66/S Fourier transform infrared spectrometer with transmittance/reflectance accessory. To avoid photoanodic dissolution of yttriumtrihydride[16] due to absorption of light with energies above 2 eV, the sample is only illuminated during the short time needed to record the spectra, typically a few seconds. Simultaneous four-point resistivity measurements are performed as described by van der Pauw[21] using a Keithley 2000 Multimeter. Details of the experimental setup were given in a previous publication.[17]

Structural measurements employing high-angle x-ray scattering are carried out in a Rigaku X-ray diffractometer, operated in the $\theta$-$2\theta$ mode using Cu $K\alpha$ radiation from a rotating anode X-ray generator ($\lambda_{\mathrm{Cu}\ K\alpha}=1.542$ nm). The measuring time for the $2\theta$-angle region $26°-36°$ is typically 10 min, to ensure good angle and time resolution. Hydrogen (un)loading is done in the gas phase. Both x-ray spectra and resistivity are recorded simultaneously as a function of time. The four-point van der Pauw method[21] for measuring resistivity allows us, despite differences in sample geometry, to link the x-ray-diffraction results to the electrochemical experiments. As described previously, this limits the error in the hydrogen concentration determination to 3%.[14,17]

The 1-M KOH electrolyte solution is prepared from *pro analysis* grade chemicals and double distilled water. Before each measurement high purity argon gas (5N) is bubbled through the solution to remove oxygen. During the experiments an argon flow is maintained over the electrolyte. All measurements are performed at room temperature.

## III. RESULTS

### A. Continuous galvanostatic loading

The result of an electrochemical loading experiment using a 300-nm-thick yttrium film capped with a 15-nm-thick palladium layer (to be referred to as 300Y/15Pd in the rest of this work) in 1-M KOH is shown in Fig. 1. A constant current $|j|=0.2$ mA/cm$^2$ ($j<0$ is the absorption, and $j>0$ is the desorption) is applied, resulting in a linear variation of the hydrogen concentration with time. Figure 1(a) shows the optical transmittance at 1.96 eV. Two branches are observed: the lower one for the case of hydrogen absorption, and the higher one for desorption. With increasing hydrogen concentration the transmittance first decreases and reaches a minimum at $x=2.1$. This decrease has been reported previously.[7,8,14,16–18] Upon further loading the transmittance increases strongly to finally reach a constant value at $x>2.8$. In the case of desorption the transmittance characteristics are markedly different. Starting at maximum hydrogen concentration the transmittance first drops to about 10%, exhibits a humplike feature at $x\approx 2.65$, and then decreases monotonically to the stable dihydride state. The minimum at $x=2.1$ is not observed. When during hydrogen loading the current is reversed at intermediate concentrations, the transmittance immediately starts to rise until it reaches the desorption branch which it then follows. Similarly, when changing from desorption to absorption the transmittance decreases and joins the absorption branch. Variation of the absorption and desorption rate by changing the current density has no marked influence on the aforementioned behavior. Moreover, identical results are obtained from a potentiodynamic measurement in which the potential is scanned at a rate as low as 0.1 mV/s. Also, increasing the temperature up to 70 °C does not lead to a significantly different behavior of the transmittance characteristics.

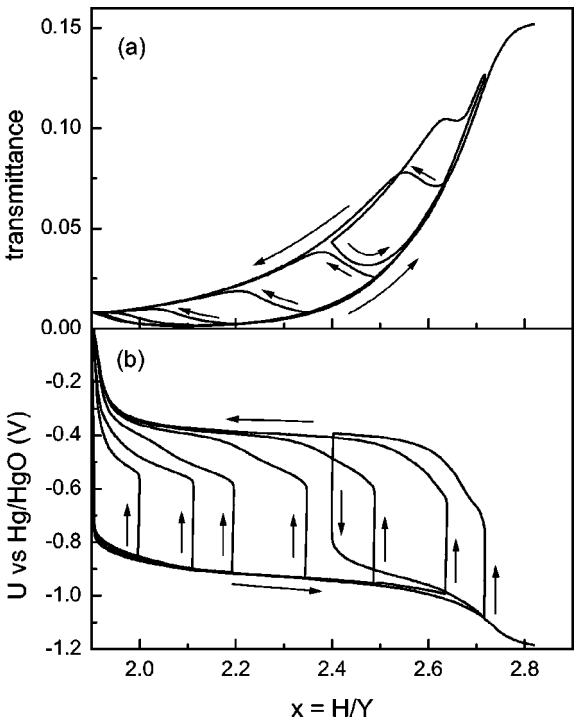


FIG. 1. (a) Optical transmittance at 1.96 eV and (b) electrode potential as a function of hydrogen concentration $x$ for a 300Y/15Pd film in 1-M KOH during a galvanostatic loading experiment. The (un)loading current amounted to $(+)-0.2$ mA/cm$^2$. The arrows indicate whether hydrogen is absorbed or desorbed.

The potential measured during hydrogen cycling described above is shown in Fig. 1(b). Upon loading with hydrogen the potential drops from 0 to $-0.8$ V almost immediately. Between $x=2.1$ and 2.6 the potential decreases slowly, followed by a more rapid decline to a value near

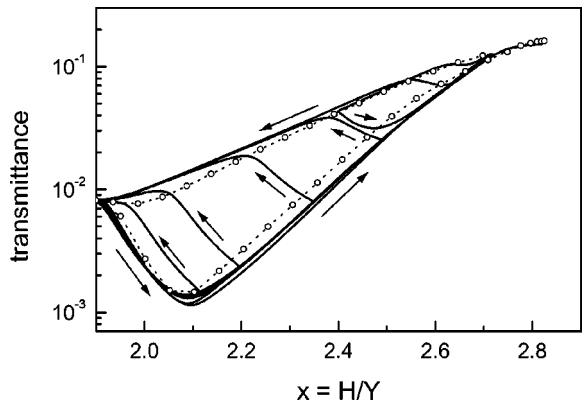


FIG. 2. Optical transmittance at 1.96 eV as a function of the hydrogen concentration $x$ for a 300Y/15Pd film. The solid line is identical to the result of Fig. 1(a), but now on a logarithmic scale. Additionally, the result of a measurement using the galvanostatic intermittent titration technique is shown (○, dashed curve). The equilibrium absorption results at high hydrogen concentrations are corrected for the overestimate of $x$ due to hydrogen gas evolution.

$-1.2$ V. At $x=2.6$ hydrogen gas evolution at the electrode surface ($H_2O+e^- \rightarrow \frac{1}{2}H_2+OH^-$) starts to compete with hydrogenation of the yttrium film. The consumption of charge carriers in the formation of $H_2$ becomes increasingly more important at negative potentials; when the potential reaches a constant value near $-1.2$ V, no more hydrogen is absorbed in the film. During hydrogen desorption, starting at any concentration, the potential rises slowly in the concentration range where the transmittance increases from the absorption to the desorption branch in Fig. 1(a). Once the desorption curve in transmittance is reached, the potential remains approximately constant at $U=-0.4$ V, to finally rise to values $U>0$ V toward $x=1.9$. When the current is reversed at an arbitrary concentration either during absorption or desorption, a potential step of approximately 0.35 V is observed, which is due to the fact that the cell potential $U$ is a sum of the equilibrium potential $U_{eq}$ and an extra potential $\Delta U$. The latter is a result of charge transfer at the solid/electrolyte interface, which introduces an overpotential $\eta$, and the Ohmic potential ($iR$) drop in the electrolyte. In contrast to the transmittance characteristics, the potential depends strongly on temperature and applied current density. At lower current densities and/or elevated temperatures the difference between the loading and unloading potentials decreases significantly. This is evident as the $iR$ drop is directly related to the current density, and the overpotential $\eta$ depends on both current density and temperature.

In Fig. 2 the transmittance of Fig. 1(a) is shown on a logarithmic scale. The large difference between absorption and desorption is more pronounced, especially at low concentrations. For a full absorption and desorption cycle three regimes can be distinguished in which the logarithm of the transmittance ($\ln T$) varies approximately linearly with concentration: (i) during absorption between $x=1.9$ and 2.1, the transmittance decreases by about one order of magnitude; (ii) this is followed by a strong increase of the transmittance over more than two orders of magnitude; and (iii) during desorption a linear decrease of $\ln T$ is observed. Although less pronounced, the linear behavior of $\ln T$ is also observed during transitions between the absorption and desorption branches at intermediate concentrations.

### B. Equilibrium measurements

To eliminate effects related to the kinetics of hydrogenation we employ the galvanostatic intermittent titration technique (GITT) to study the physical properties of our electrochemically loaded switchable yttrium hydride films under equilibrium conditions.[17] In the GITT a constant current is applied for some time to change the hydrogen concentration by a certain amount. Whether hydrogen is absorbed or desorbed depends on the sign of the current. After this pulse the current is interrupted, and the system relaxes under open-circuit conditions, while the potential, resistivity and optical transmittance and reflectance are monitored *in situ*. As mentioned in previous publications, the relaxation kinetics are surprisingly slow,[16,17] the origin of which is uncertain, and which will be the subject of future work. The concentration dependence of the aforementioned physical quantities is determined using the values obtained at the end of the equilibration period. In Fig. 2 the optical transmittance at 1.96 eV measured using the GITT is compared to what is found during continuous galvanostatic loading. Although the hysteresis between the absorption and desorption is slightly less, essentially the same features are observed. The minimum at $x=2.1$ during hydrogen loading is absent in unloading; the three linear regimes are clearly observed. When switching from the absorption curve to the desorption curve, and vice versa, identical behavior is found as during the continuous loading experiments (not shown in Fig. 2). As the hysteresis in the optical transmittance observed under equilibrium conditions is very similar to the result of the continuous (un)loading experiment, the hysteretic behavior is not related to the slow kinetics of the system.

From the equilibrium potential $U_{eq}$ an equivalent hydrogen pressure $p_{H_2}$ (bar) is calculated using the Nernst equation

$$\ln p_{H_2} = -\frac{2F}{RT}(U_{eq}+0.926), \tag{2}$$

where $R=8.314$ J/K mol is the gas constant, and $F=96485$ C/mol is the Faraday constant. This enables us to construct the pressure-composition isotherm for the yttrium-hydrogen system between dihydride and trihydride, both during hydrogen absorption and desorption. The result for a 300Y/15Pd film in 1-M KOH is shown in Fig. 3. In absorption first a strong increase is observed between $x=1.9$ and 2.1, followed by a much slower, almost linear increase of the logarithm of the pressure with hydrogen concentration from $p_{H_2}=3.2\times10^{-7}$ bar at $x=2.1$ to $p_{H_2}=1.5\times10^{-5}$ bar at $x=2.55$. At $x$ values above 2.6 the pressure again increases more rapidly to end at $p_{H_2}=1$ bar. This is the maximum attainable pressure value for a hydrogen-metal system in equilibrium at an ambient pressure of 1 bar. As described in Sec. III A, competition between hydrogenation of the film and hydrogen gas evolution leads to an increasing overestimate of the hydrogen concentration; the data are corrected for this overestimate by assuming an exponential potential dependence of the kinetics for hydrogen gas evolution near $-0.926$ V. A

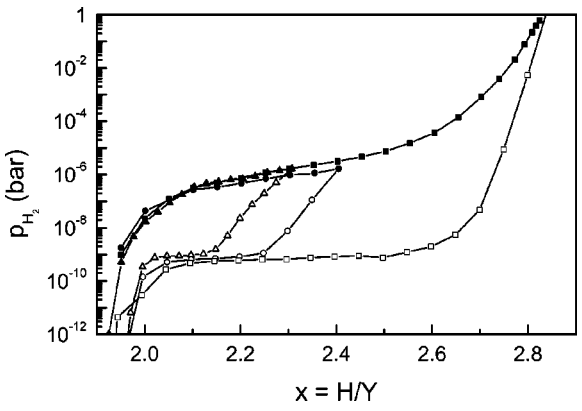


FIG. 3. Pressure-composition isotherm of a 300Y/15Pd film. Measurements were performed using the galvanostatic intermittent titration technique. The filled and open symbols pertain to hydrogen absorption and desorption, respectively. The absorption results at high hydrogen concentrations are corrected for the overestimate of $x$ due to hydrogen gas evolution.

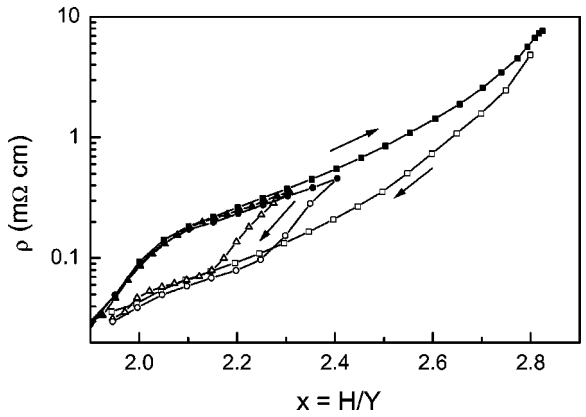


FIG. 4. Resistivity as a function of hydrogen concentration $x$ for a 300Y/15Pd film. Measurements were performed using the galvanostatic intermittent titration technique. The filled and open symbols pertain to hydrogen absorption and desorption, respectively. The absorption results at high hydrogen concentrations are corrected for the overestimate of $x$ due to hydrogen gas evolution. The resistivity values are corrected for the palladium cap layer.

full desorption isotherm is shown by the open squares in Fig. 3. After a sharp decrease of the pressure, an almost flat plateau is found between $x=2.6$ and 2.0 at $p_{H_2}=7.5\times10^{-10}$ bar. Toward $x=1.9$ the pressures again decreases very rapidly. When starting to desorb hydrogen at intermediate concentrations (open circles and triangles), a similar pressure drop is observed until the plateau is reached, and the pressure then exhibits the same characteristics as for a full desorption.

From the plateau pressure corresponding to a coexistence region between two phases ($\beta$ and $\gamma$ in our case) we can calculate the enthalpy of formation $\Delta H_f$ using the relation[22,23]

$$\ln p_{H_2}=\frac{2\Delta H_f}{RT}+\frac{S^0_{H_2}}{R}, \tag{3}$$

where $S^0_{H_2}=130.8$ J/K mol $H_2$ is the standard molar entropy of hydrogen gas. From the desorption plateau we obtain $\Delta H_f=-44.8$ kJ/mol H. Considering that Eq. (3) underestimates $\Delta H_f$, this value is in reasonable agreement with the value $\Delta H_f=-41.8$ kJ/mol H, as determined by Flotow *et al.*[24] Yannopoulos *et al.*[25] measured isotherms in the range 250–350 °C, and from a fit to the plateau pressure as a function of temperature $\Delta H_f=-43.1$ and $-42.2$ kJ/mol H are obtained for absorption and desorption, respectively. From the absorption isotherm we can estimate the partial molar enthalpy to have a value between $\Delta\bar{H}=-37.4$ and $-32.7$ kJ/mol H by taking the pressure values $p_{H_2}=3.2\times10^{-7}$ bar and $p_{H_2}=1.5\times10^{-5}$ bar at $x=2.1$ and 2.55, respectively. These enthalpies are significantly higher than the values mentioned above for the case of hydrogen desorption. For comparison, from an absorption isotherm, measured by means of a quartz-crystal microbalance, Huiberts *et al.*[20] found a sloping plateau around $p_{H_2}=9.21\times10^{-5}$ bar, from which they obtain a formation enthalpy $\Delta\bar{H}=-30.0$ kJ/mol H.

The resistivity, measured simultaneously with the pressure-composition isotherms in Fig. 3, is plotted in Fig. 4. The resistivity $\rho=29$ $\mu\Omega$ cm in the desorbed dihydride state at $x=1.9$ corresponds to the minimum value measured in a first loading experiment using an as-deposited sample.[17] An increase of the hydrogen concentration results in a sharp rise of the resistivity followed by a characteristic kink near $x=2.04$ at $\rho\approx0.14$ m$\Omega$ cm, after which the resistivity increases further to reach a final value $\rho=7.8$ m$\Omega$ cm. The resistivity values are corrected for the short circuit through the palladium cap layer using the parallel resistor model for the 15-nm-thick palladium layer and the 300-nm-thick yttrium layer.[26] When approaching $x=3$ this shunting effect becomes increasingly more important, owing to the strong rise of the resistivity of substoichiometric yttrium trihydride in this concentration range.[17] When desorbing hydrogen from the film the measured resistivity values are markedly lower, leading to hysteresis in the electrical characteristics. Furthermore, the kink which was observed in absorption is hardly discernible upon unloading. Similar to what has been described for the transmittance and the pressure-composition isotherms, when starting desorption or absorption at intermediate hydrogen concentrations a transition is seen from the top to the bottom branch, or vice versa (the latter is not shown in Fig. 4).

### C. X-ray diffraction

Bulk yttrium crystallizes in the hexagonal close-packed (hcp) structure, which upon hydrogenation transforms to the face-centered cubic (fcc) structure in the dihydride state. At even higher hydrogen concentrations towards the trihydride state a second crystallographic phase transition brings the system back to the hcp structure.[27,28] More precisely, by means of neutron diffraction $YH_3$ was shown to have a $HoD_3$ ($P\bar{3}c1$) structure,[29,30] but the small displacements of the yttrium atoms and the positions of the hydrogen atoms are not visible in x-ray diffraction. As the structural properties of $YH_x$ films may differ from those available in the literature (which are only for bulk or powder samples) we carried out a detailed investigation by means of *in situ* x-ray diffraction on $YH_x$ films loaded from the gas phase. As de-

TABLE I. Lattice constants for bulk yttrium, yttrium dihydride, and yttrium trihydride reported in literature. Also given are the calculated distances $d_\perp$ and $d_\parallel$ between the hexagonal planes and the nearest-neighbor distance within these planes, respectively. In the last column the molar $YH_x$ volume is listed.

| | Ref. | $a$ (Å) | $c$ (Å) | $d_\perp$ (Å) | $d_\parallel$ (Å) | $\overline{V}_{YH_x}$ ($cm^3$) |
|---|---|---|---|---|---|---|
| hcp Y | 31 | 3.650 | 5.737 | 2.8685 | 3.650 | 19.924 |
| fcc $YH_2$ | 32 | 5.199 | - | 3.0016 | 3.6762 | 21.149 |
| | 33 | 5.205 | - | 3.0051 | 3.6805 | 21.222 |
| | 34 | 5.201 | - | 3.0028 | 3.6777 | 21.174 |
| | 35 | 5.209 | - | 3.0074 | 3.6833 | 21.272 |
| Average | | 5.2035 | - | 3.0042 | 3.6794 | 21.204 |
| hcp $YH_3$ | 33 | 3.672 | 6.659 | 3.3295 | 3.672 | 23.405 |
| | 34 | 3.674 | 6.599 | 3.2995 | 3.674 | 23.220 |
| | 24 | 3.672 | 6.625 | 3.3125 | 3.672 | 23.285 |
| Average | | 3.6727 | 6.6277 | 3.3140 | 3.6727 | 23.304 |

scribed in Sec. II, the results are mapped onto the electrochemical results via the electrical resistivity, which is measured simultaneously in the x-ray experiment and in the electrolytical/optical experiments described in the previous sections, thereby giving the concentration dependence of the crystallographic structure. To obtain even more direct information on this hydrogen concentration dependence, we plan to perform an *in situ* study of the crystallographic structure of electrochemically loaded $YH_x$ films using synchrotron radiation.

Although our molecular-beam-epitaxy-grown films are polycrystalline, they show a preferential orientation with the [002] direction ($c$ axis) perpendicular to the substrate, or in other words, with the hexagonal basal planes of the hcp unit cell parallel to the substrate. Upon hydrogenation a reordering of the hexagonal planes yields the fcc structure with the [111] direction perpendicular to the substrate. In Table I bulk literature values for the lattice constants of $YH_x$ are summarized. Also given are the separation $d_\perp$ between consecutive hexagonal planes (hcp: $d_\perp = c/2$; fcc: $d_\perp = a/\sqrt{3}$), the nearest-neighbor distance $d_\parallel$ within these planes (hcp: $d_\parallel = a$; fcc: $d_\parallel = a/\sqrt{2}$) and the molar yttrium volume $\overline{V}_Y$. Upon hydrogenation the major expansion is along the original $c$ axis (4.7% between Y and $YH_2$ and 10.3% between $YH_2$ and $YH_3$), while the maximum $a$-axis change is limited to 0.8%. This implies that in a crystallographic study of the $YH_x$ system we can focus on a narrow $2\theta$ range (26°–32°) containing only the (002) hcp Y, (111) fcc $YH_2$, and (002) hcp $YH_3$ reflectance peaks. Experimentally obtained lattice constants are listed in Table II. The lattice constant of our as-grown yttrium is slightly larger than that reported for bulk material; this is in agreement with the as-deposited initial hydrogen concentration $x \approx 0.08$ as found by Huiberts *et al.*[20] The out-of-plane expansion amounts to 4.2% between Y and $YH_2$ and 10.0% between $YH_2$ and $YH_3$, which is slightly smaller than for bulk material. The in-plane expansion toward $YH_{3-\delta}$ is larger than what is found for bulk material.

The result of an x-ray experiment on a 300Y/15Pd film loaded from the gas phase is shown in Fig. 5. As mentioned before, we only focus on the concentration range between the dihydride and trihydride configurations. The inset shows three diffraction spectra obtained in the dihydride phase (solid line), the trihydride phase (dotted line), and at an intermediate hydrogen concentration (dashed line). Two peaks at $2\theta = 26.97°$ and 29.68° correspond to the (111) fcc $YH_2$ and (002) hcp $YH_3$ reflectances, respectively. In Fig. 5 the intensity ratio $\eta = I_{YH_3(002)}/I_{YH_2(111)}$ is plotted as a function of hydrogen concentration during absorption and desorption. These data reveal a most remarkable behavior of $YH_x$ films during hydrogen loading and unloading. Upon hydrogen loading the intensity ratio $\eta$ increases by five orders of magnitude, indicating a rapid transformation from fcc to hcp. This transformation is essentially complete at $x \approx 2.15$. Above $x = 2.15$, $YH_x$ is therefore in a hcp phase in sharp contrast with bulk $YH_x$. Upon hydrogen desorption the fcc phase immediately precipitates at high hydrogen concentrations $x$. All the way down to the stable dihydride configuration the two crystallographic phases coexist as observed in bulk samples.

TABLE II. Experimentally determined lattice constants of a 300-nm Y, 15-nm Pd film loaded from the gas phase. As in Table I, the calculated distances $d_\perp$ and $d_\parallel$ between the hexagonal planes and the nearest-neighbor distance within these planes, as well as the molar $YH_x$ volume, are given.

| | $a$ (Å) | $c$ (Å) | $d_\perp$ (Å) | $d_\parallel$ (Å) | $\overline{V}_{YH_x}$ ($cm^3$) |
|---|---|---|---|---|---|
| hcp Y | 3.662 | 5.770 | 2.885 | 3.662 | 20.170 |
| fcc $YH_2$ | 5.206 | - | 3.006 | 3.681 | 21.235 |
| hcp $YH_{2.2}$ | 3.713 | 6.613 | 3.307 | 3.713 | 23.766 |
| hcp $YH_3$ | 3.713 | 6.612 | 3.306 | 3.713 | 23.762 |

This hysteretic behavior is also clearly observed in Fig. 6, which shows contour plots of concentration-dependent x-ray spectra during hydrogen absorption and desorption. The two intensity maxima at $2\theta = 26.97°$ and 29.68° were described

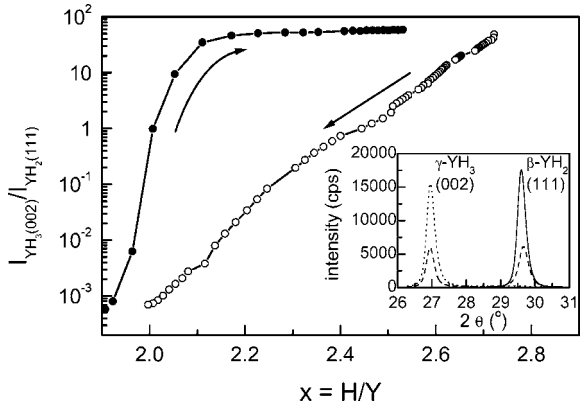


FIG. 5. Intensity ratio of the (002) and (111) x-ray-diffraction peaks of hcp $YH_3$ and fcc $YH_2$, respectively, as a function of hydrogen concentration $x$ during a gas phase loading experiment using a 300Y/15Pd film. Spectra were measured as a function of resistivity; the corresponding hydrogen concentration was obtained from the results in Fig. 4. The filled and open symbols pertain to hydrogen absorption and desorption, respectively. The inset shows three diffraction spectra obtained in the fcc $\beta$ phase (solid line; $x = 2.0$), in the $\beta$-$\gamma$ two-phase region (dashed line; $x = 2.4$ during desorption), and in the hcp $\gamma$ phase (dotted line; $x = 2.7$).

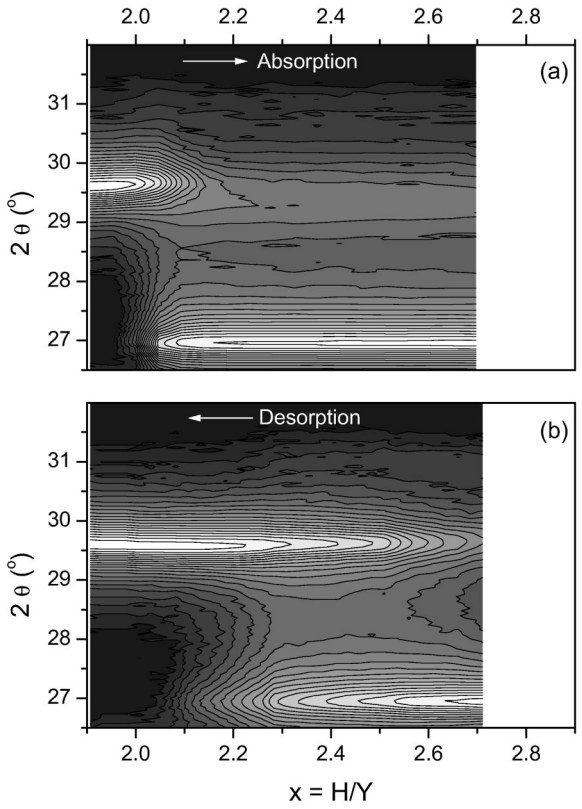


FIG. 6. Contour plots of the x-ray intensity as a function of hydrogen concentration $x$ during absorption (a) and desorption (b). The grayscale corresponds to a logarithmic intensity scale.

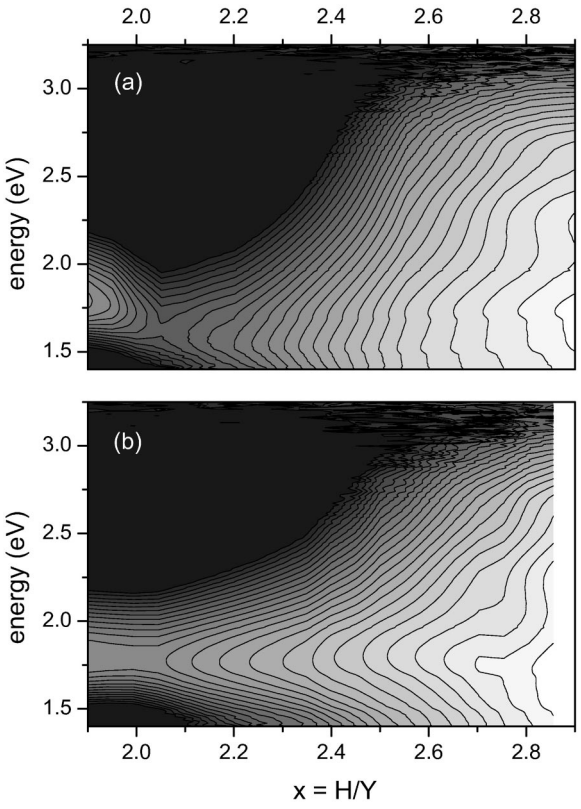


FIG. 7. Contour plots of the optical transmittance for an electrochemically loaded 300Y/15Pd film as a function of the hydrogen concentration $x$ during hydrogen absorption (a) and desorption (b). The step size was $\Delta x = \pm 0.05$. The lightest regions correspond to a maximum transmittance of approximately 18%. The grayscale corresponds to a logarithmic intensity scale.

above. The weak intensity maximum near $2\theta = 29.25°$ corresponds to the (101) hcp $YH_3$ reflectance. Due to the logarithmic grayscale, this small peak is greatly enlarged. There is no discernible shift of the peaks in both fcc $YH_2$ and hcp $YH_3$ phases, either during absorption or desorption. This is especially surprising during absorption as it implies that above $x = 2.15$ the $c$ axis of the single hcp phase does not expand during hydrogen uptake up to $x = 2.8$.

### D. Optical spectroscopy

The GITT allows us to simultaneously perform optical transmittance and reflectance measurements. At the end of every equilibration period, transmittance and reflectance spectra are recorded. Figure 7 shows contour plots of the transmittance as a function of hydrogen concentration during electrochemical absorption (a) and desorption (b). In Fig. 8, spectra of the optical transmittance during loading (a) and unloading (b) in the low concentration range ($1.9 \leqslant x \leqslant 2.3$) are presented. Clearly, there are marked differences between hydrogen absorption and desorption. The dihydride transmittance window, with a maximum transmittance of approximately 1.3% at a photon energy $E_{ph} = 1.8$ eV, shifts to lower energy ($E_{ph} = 1.6$ eV at $x = 2.1$), while the maximum intensity drops to 0.35%. After the minimum at $x = 2.1$ toward fully loaded trihydride the transmittance increases exponentially over a wide spectral range ($1.4 \leqslant E_{ph} \leqslant 3.0$ eV), similar to what was observed in Figs. 1 and 2 at a photon energy $E_{ph} = 1.96$ eV.

In desorption a similar exponential decrease is also observed, but now all the way down to the low concentration limit; no minimum is observed. Moreover, already at relatively high concentrations ($x \approx 2.6$) the characteristic dihydride maximum can be discerned at $E_{ph} = 1.8$ eV. Also, there is no marked shift of this maximum, as was the case during absorption between $x = 1.9$ and 2.1. When desorption is started at intermediate concentrations [Fig. 8(b)] the transmittance characteristics immediately show a transition to dihydridelike behavior with a peak near $E_{ph} = 1.8$ eV. The intensity maximum at $x = 2.18$ (curve 6, peak intensity 1.6%) is followed by a decrease of the intensity over the entire spectral range. As in the contour plot of Fig. 7, there is no marked shift of the transmittance peak in Fig. 8(b). Close to the lowest attainable hydrogen concentration, the spectrum (curve 8) has a slightly lower transmittance (1.2%) than the final dihydride transmittance.

In Fig. 9 contour plots of the optical reflectance as a function of hydrogen concentration are presented for absorption (a) and desorption (b). Figure 10 shows reflectance spectra during loading (a) and unloading (b) in the low concentration range ($1.9 \leqslant x \leqslant 2.3$), corresponding to the optical transmittance spectra of Fig. 8. Although less pronounced, the reflectance also exhibits hysteresis. The strong reflectance of $YH_2$ below the apparent plasma energy at $E_{ph} = 1.6$ eV is related to the number of free charge carriers, while the features at higher photon energies are related to interband transitions. A more detailed description of the relation between optical properties and electronic band structure will be given else-

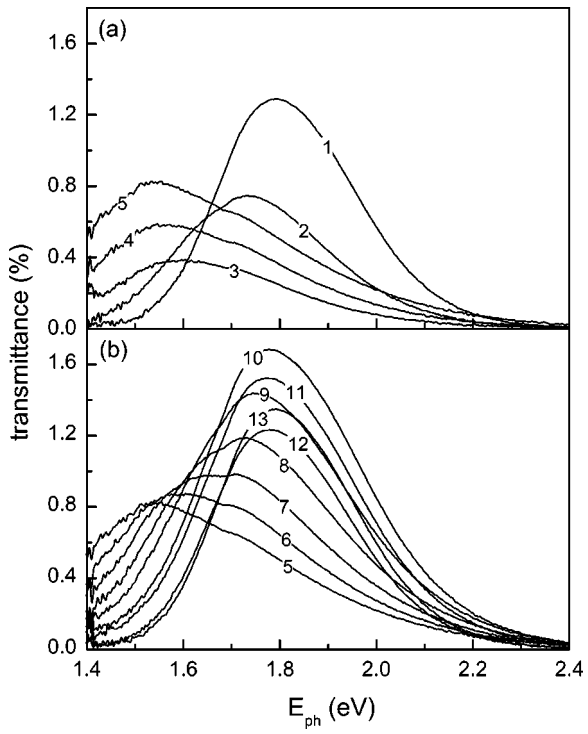


FIG. 8. (a) Optical transmittance spectra for an electrochemically loaded 300Y/15Pd film during hydrogen absorption. The numbers 1–5 correspond to hydrogen concentrations $x=1.9$, 2.0, 2.1, 2.2, and 2.3, respectively. (b) Same as in (a), but now during hydrogen desorption started at $x=2.3$. The numbers 5–13 correspond to concentrations $x=2.3$, 2.28, 2.25, 2.23, 2.2, 2.18, 2.1, 2.0, and 1.95, respectively.

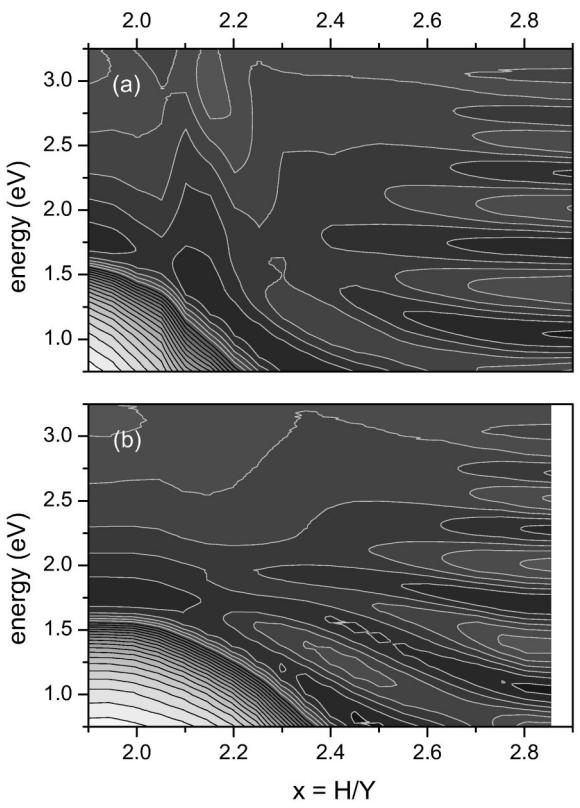


FIG. 9. Contour plots of the optical reflectance for an electrochemically loaded 300Y/15Pd film as a function of the hydrogen concentration $x$ during hydrogen absorption (a) and desorption (b). The step size was $\Delta x=\pm 0.05$. The lightest regions correspond to a maximum reflectance of approximately 85%. The grayscale corresponds to a linear intensity scale.

where. From Fig. 9(a) it is clear that upon hydrogenation the free-electron reflectance shifts to lower energy, indicating a lowering of the free charge-carrier density. At hydrogen concentrations above $x=2.3$ the free-electron contribution has moved out of the detection range. At higher hydrogen concentrations ($x\geqslant 2.5$) the spectra exhibit characteristics of a transparent insulator. The reflectance is low ($<25\%$), and interference of the light reflected at the palladium/yttrium interface and the yttrium/substrate interface is observed. Absorption above the optical gap of 2.8 eV results in a strong diminishing of these interference fringes, in agreement with the decline of the transmittance in the same energy range (Fig. 7).

Desorption of hydrogen leads to a decrease of the interference pattern and results in a reappearance of the low-energy reflectance. However, this free-electron contribution is already observed at $x=2.4$, and the onset of this reflectance is always at higher photon energy than during absorption at corresponding $x$ values [compare Figs. 9(a) and 9(b)]. This is in qualitative agreement with the resistivity data of Fig. 4, since the average plasma energy $\hbar\omega_p$ is related to the average density of free electrons $n$ through $\omega_p^2=ne^2/\varepsilon_0 m^*$, where $e$, $\varepsilon_0$, and $m^*$ are all constants.[36] Assuming that we can envisage the $YH_x$ system in terms of an effective medium, both the higher plasma energy $\hbar\omega_p$ and the lower resistivity observed during hydrogen desorption indicate a larger overall number of free charge carriers.

## IV. DISCUSSION

Since the large hysteresis reported in Sec. III is related to the intrinsic difference between single hcp $YH_x$ synthesized during hydrogen absorption and mixed-phase $YH_x$ during desorption, we discuss hydrogen absorption and desorption separately, starting with hydrogen desorption since it behaves very similarly to bulk (or powder) $YH_x$.

### A. Hydrogen desorption

The characteristics of thin $YH_x$ films described in this work during *desorption* from trihydride to dihydride show strong similarities with what has been reported for bulk material. From the x-ray-diffraction results in Figs. 5 and 6(b), it is clear that from $x=2.7$ down to 2.0 fcc $YH_{2+\delta}$ and hcp $YH_{3-\delta}$ phases coexist. Further evidence for the coexistence of the two phases is given by the pressure-composition isotherm in Fig. 3, which exhibits a plateau in the same concentration range. The limiting hydrogen concentrations of the two-phase region are in reasonable agreement with the values found for bulk $YH_x$.[27] Moreover, the heat of formation estimated from our desorption isotherm is comparable to values determined by Flotow *et al.*,[24] and obtained from a fit to data measured at elevated temperatures (250–350 °C).[25]

The transmittance and the resistivity measured in the coexisting phase region are related to the optical and electrical properties of the two separate phases. The hydrogen concen-

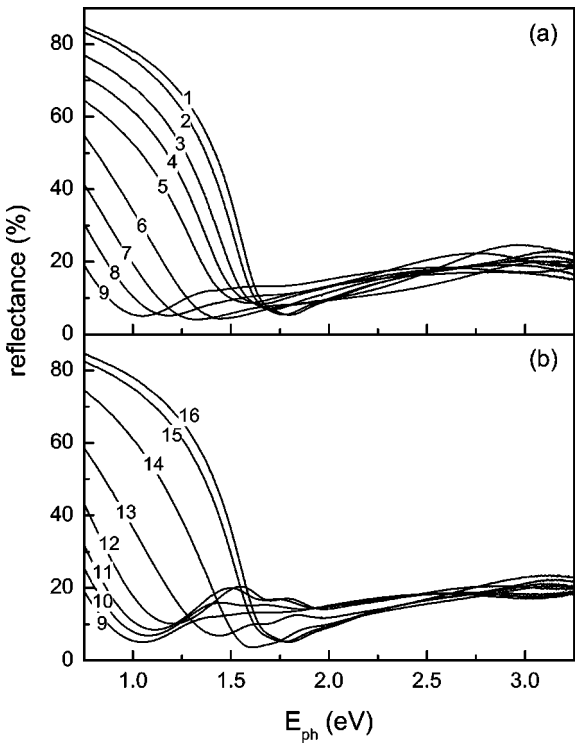


FIG. 10. (a) Optical reflectance spectra for an electrochemically loaded 300Y/15Pd film during hydrogen absorption. The numbers 1–9 denote successive spectra from $x=1.9$ to $x=2.3$ ($\Delta x=0.05$). (b) Same as in (a), but now during hydrogen desorption. The numbers 9–16 denote successive spectra from $x=2.3$ to 1.95 ($\Delta x=-0.05$).

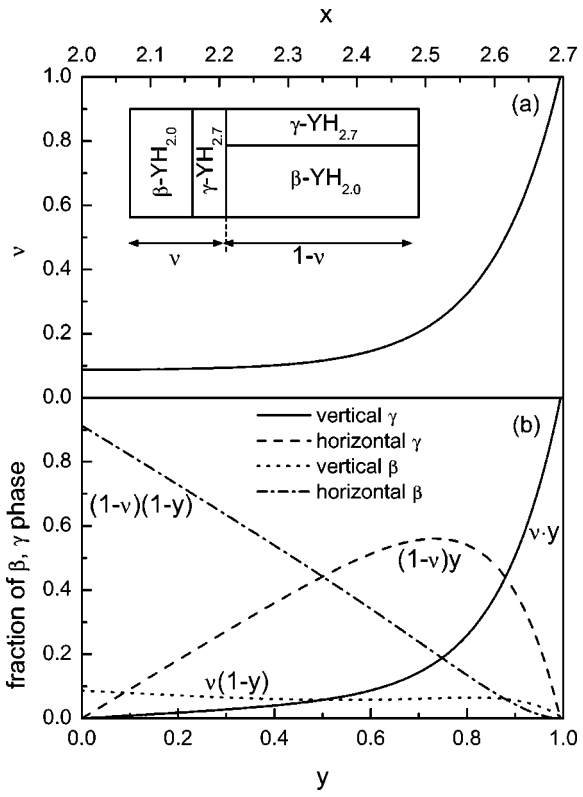


FIG. 11. (a) The function $\nu$ as a function of the scaled concentration $y=(x-2.0)/(2.7-2.0)$ in the two-phase region. The inset shows a schematic representation of various phases we used to model the experimentally observed transmittance and resistivity. (b) Fraction of the various phases as a function of the scaled hydrogen concentration, calculated using the function $\nu$.

tration dependency of both the transmittance and the resistivity can be rationalized by means of a simple model.[37] Let us assume that a fraction $\nu$ of the film consists of regions where the high concentration $\gamma$-$YH_{2.7}$ and the low concentration $\beta$-$YH_{2.0}$ coexist next to each other in a columnar way. In the rest of the film (fraction $1-\nu$) the two phases are stacked on top of each other in a layered configuration. This is schematically shown in the inset of Fig. 11(a). Considering that the current used to measure the resistivity passes through the film horizontally, while the transmitted light travels vertically, we arrive at the following expressions for the optical transmittance (using the Lambert-Beer relation) and the electrical resistivity:

$$T=\nu[(1-y)T_\beta+yT_\gamma]+(1-\nu)[(T_\beta)^{1-y}(T_\gamma)^y], \quad (4a)$$

$$\rho_{tot}=\nu[(1-y)\rho_\beta+y\rho_\gamma]+\frac{1-\nu}{\frac{1-y}{\rho_\beta}+\frac{y}{\rho_\gamma}}, \quad (4b)$$

where $T_\beta$ ($T_\gamma$) and $\rho_\beta$ ($\rho_\gamma$) represent the transmittance and resistivity of a complete $\beta$-$YH_{2.0}$ ($\gamma$-$YH_{2.7}$) layer, and $y=(x-2.0)/(2.7-2.0)$ is the overall fraction of $\gamma$-$YH_{2.7}$ phase (from Fig. 3). Using $\nu=a+b\exp(y/c)$ with $a=0.086$, $b=9.2\times10^{-4}$, and $c=0.144$ [see Fig. 11(a)], we obtain good fits to both the transmittance and the resistivity data. The results are shown in Figs. 12(a) and 12(b), where the solid lines represent calculated curves and the data points correspond to the desorption data in Figs. 2 and 4.

Using the function $\nu$ we can easily calculate the fractions of the horizontal and vertical $\beta$ and $\gamma$ phases as a function of the scaled hydrogen concentration $y$; the result is shown in Fig. 11(b). Moreover, for three values of $y$ the distribution of the phases is schematically shown in Fig. 13. It is immediately clear that at low concentrations the two phases are mainly distributed in a layered configuration; only a small fraction of the $\gamma$-$YH_{2.7}$ phase forms columnar structures through the entire thickness of the film. With increasing hydrogen content the fraction of $\beta$-$YH_{2.0}$ phase distributed in columns stays approximately constant, while the penetration of the high concentration phase through the whole film becomes considerable toward the complete $\gamma$-$YH_{2.7}$ configuration.

### B. Hydrogen absorption

As mentioned before, $YH_x$ behaves completely differently during *absorption* than bulk material. Two regimes can be distinguished during hydrogen loading. From the x-ray-diffraction results in Fig. 5 it follows that in the narrow concentration range between $x=1.9$ and 2.1 a rapid transition occurs from the cubic to the hexagonal structure. Surprisingly, at concentrations above $x=2.1$ the thin $YH_x$ film remains in the hcp phase, and does not exhibit any further expansion [Fig. 6(a)]. The separation into two absorption regimes is also apparent from the transmittance minimum at $x=2.1$ in Figs. 1 (a), 2, 7(a), and 8(a), and the sudden change of slope in the resistivity near $x=2.1$ in Fig. 4.

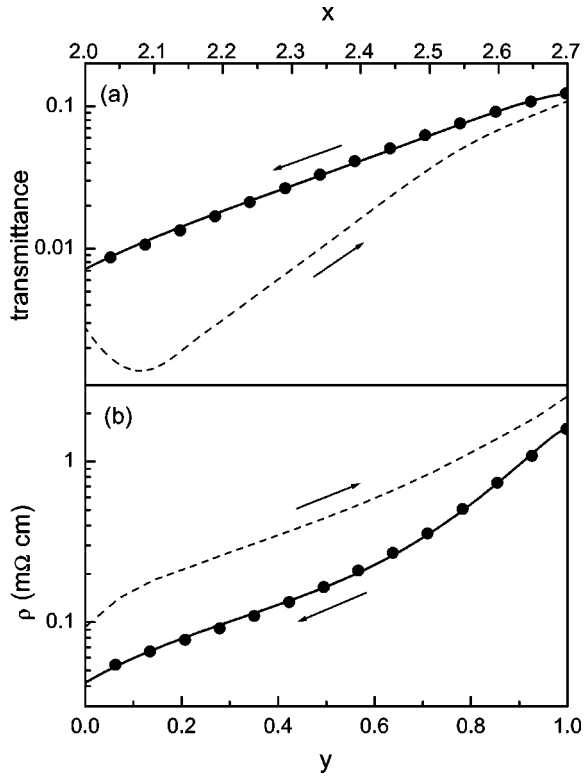


FIG. 12. Transmittance (a) and resistivity (b) in the two-phase coexistence region as a function of the scaled hydrogen concentration $y$, taken from Figs. 2 and 4. The solid lines are calculated using the model described in the text. The dashed lines represent the transmittance and resistivity during absorption, also taken from Figs. 2 and 4.

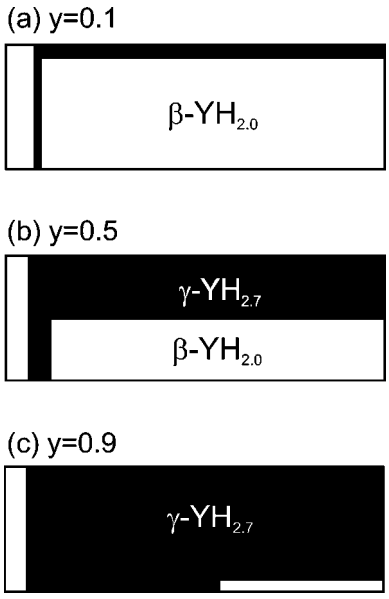


FIG. 13. Schematic illustration of the distribution of the $\beta$-$YH_{2.0}$ and $\gamma$-$YH_{2.7}$ phases within the film at three hydrogen concentrations: (a) $y=0.1$, (b) $y=0.5$, and (c) $y=0.9$. The black and white regions represent the $\gamma$-$YH_{2.7}$ and $\beta$-$YH_{2.0}$ phases, respectively. Note that in reality the columnar and layered regions will be randomly distributed throughout the sample.

In the two-phase region ($1.9 \leqslant x \leqslant 2.1$) the approximately linear decrease of $\ln T$ with hydrogen concentration can be understood in terms of a similar model as described for the case of hydrogen desorption, but now with a moderately transparent ($\sim 1\%$) fcc phase and a much more opaque low-concentration hcp phase. Furthermore, up to $x=2.1$ the transmittance spectra exhibit a maximum which shifts slightly to lower energy [Fig. 7(a)], but is still reminiscent of the characteristic dihydride transmittance. To our surprise, the pressure-composition isotherm in Fig. 3 does not show a plateau for $1.9<x<2.1$. Also, the dynamic results of Fig. 1(b) do not indicate a plateau in this concentration range, but merely a difference in slope below and above $x=2.1$.

At first sight it is rather surprising that in the single hcp phase the crystal lattice does not show any expansion [Fig. 6(a)] over the entire concentration range between $2.1 \leqslant x \leqslant 2.8$. However, this constancy of the lattice spacing is consistent with calculations of Chou *et al.*[38] for various phases of $YH_x$ between the dihydride and trihydride phases. The molar volume decreases smoothly by less than 1%. This behavior is also similar to $LaH_x$,[27] which remains in the fcc phase for all $x>2$. Most fascinating for the fundamental understanding of switchable mirrors is that the metal-insulator transition, which is seen in the concentration dependency of the transmittance, reflectance, and resistivity, occurs completely within a single hcp phase. For $x>2.1$, $YH_x$ is thus one of the few systems with a continuous metal-insulator transition. Compared to other such systems [Si:P (Ref. 39) and $NiSe_{2-x}S_x$ (Refs. 40 and 41)], $YH_x$ has the advantage that the concentration of one of its constituents (hydrogen) can be varied continuously *in situ*. Furthermore, the above indicates that the metal-insulator transition in $YH_x$ is not due to a structural phase transition. In this sense $YH_x$ resembles $LaH_x$ and $Y_{1-y}Mg_yH_x$ alloys. In a recent study[13,42] it was found that, with more than 10% magnesium, the cubic fcc $YH_2$ phase in these alloys is stabilized, i.e., a structural phase transition is absent. Nevertheless, similar to $YH_x$ and $LaH_x$, the $Y_{1-y}Mg_yH_x$ alloys exhibit dramatic changes in their optical and electrical properties when the hydrogen concentration is varied. This implies that the metal-insulator transition in $RH_x$ systems is merely driven by the variation of the hydrogen concentration. It is, however, conceivable that it is accompanied by an ordering within the hydrogen sublattice.[43,44]

The concentration dependence of the electrical resistivity (Fig. 4) and the optical transmittance (Fig. 2) in the single phase region ($x>2.1$) can be interpreted in terms of a description given by Ng *et al.* for $LaH_x$.[45,46] In their work $LaH_3$ is described as an insulator, in which the hydrogen bandwidth is markedly decreased by strong electron correlation effects. The removal of neutral hydrogen atoms from the octahedral sites (or in-plane and near-plane sites in hcp $YH_x$) introduces vacancies, which effectively donate an electron to the conduction band. The strongly localized nature of these electronic vacancy states leads to the formation of an impurity band at very high doping levels of about 20%. Upon lowering the hydrogen concentration the vacancy concentration rises, and the overlap between the impurity states increases substantially. This leads to a higher mobile charge-carrier density and thus to a lower resistivity, in qualitative agreement with the result of Fig. 4.

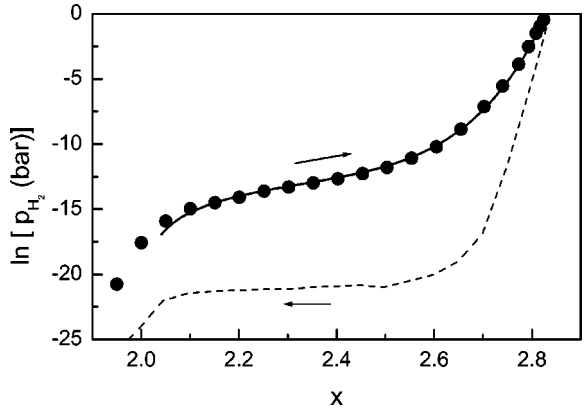


FIG. 14. Logarithm of the hydrogen pressure as a function of the hydrogen concentration. The data points are identical to the absorption isotherm in Fig. 3. The solid line is a fit to the data as described in the text. The dashed line represents the desorption isotherm of Fig. 3.

The linear $\ln T$-$x$ relationship in the single phase region in Fig. 2 can also be understood in terms of the model by Ng *et al.*[45,46] described above. When we assume that an optical extinction coefficient $\varepsilon_i$ is associated with the aforementioned vacancy state, and consider all other contributions to the optical absorption to be independent of the hydrogen concentration $x$, the transmittance is given by

$$T_{YH_x} = T_0 \exp[-\varepsilon_i (3-x) N_{YH_3} d], \tag{5}$$

in which $T_0$ and $\varepsilon_i$ are constant, $N_{YH_3}$ is the yttrium density in $YH_3$ and $d$ is the thickness of the film. Additionally, based on their theoretical calculations, Ng *et al.*[46] found that the optical absorbance due to the hydrogen vacancy states is essentially independent of the photon energy. This is indeed observed in Fig. 7(a) by the increase of the transmittance over the entire spectral range with increasing concentrations above $x=2.1$.

The absence of a plateau for $x>2.1$ in the absorption isotherm in Fig. 3 is also in agreement with a single-phase region. Starting from the lattice-gas model as described by Lacher,[47] we can estimate the effective H-H interaction from the pressure-composition isotherm. Within this simple model the hydrogen gas pressure and the hydrogen concentration in the film are related by

$$\ln \frac{p}{p_0(T)} = 2 \ln\left[\frac{x-2}{3-x}\right] + \frac{2\Delta\overline{H}(x)}{kT}, \tag{6}$$

where $\Delta\overline{H}(x)$ is the concentration dependent formation enthalpy, and $p_0(T)$ depends only on temperature. A good fit to the absorption isotherm was obtained (see Fig. 14) using a formation enthalpy of the form

$$\Delta\overline{H}(x) = \Delta\overline{H}(2) + a(x-2) + b(x-2)^c, \tag{7}$$

with $a=-47$ meV, $b=380$ meV, and $c=5.6$. The linear term in Eq. (7) is generally assumed to consist predominantly of an elastic contribution $\Delta\overline{H}_{\text{elastic}}(x)$ to the formation enthalpy, while the last term can be considered to represent the additional H-H interactions, possibly of electronic nature.[48] The value $a=-47$ meV indicates an attractive but weak elastic H-H interaction. Due to the large exponent $c$, the critical temperature is essentially given by $T_c=-a/4k$, which amounts to $T_c=136$ K. Unfortunately, at this temperature electrolytical (or gaseous) loading is not possible. The low value $a=-47$ meV compared to, for example, Pd ($-529$ meV)[48] and Nb ($-280$ meV),[48] is consistent with the essentially zero lattice expansion in $YH_x$ for $x>2.1$ (see Fig. 6 and Table II), since the elastic contribution is given by[23]

$$\frac{d\Delta\overline{H}_{\text{elastic}}}{dx} = -B\overline{V}_H \frac{d\ln V}{dx} = -B\frac{(\overline{V}_H)^2}{\overline{V}_{YH_x}}, \tag{8}$$

where $B$ represents the bulk modulus, $\overline{V}_H$ is the molar volume of hydrogen, and $\overline{V}_{YH_x}$ is the molar volume of $YH_x$. The absence of any lattice expansion in $YH_{x>2.1}$ implies an even smaller elastic H-H interaction, indicating that the linear term in Eq. (7) may also be ascribed to an electronic H-H interaction.

### C. Hysteresis

The differences in hydrogen absorption and desorption, described in the previous sections, result in considerable hysteresis in the $YH_x$ thin-film system. The optical transmittance, pressure, resistivity and crystallographic structure shown in Figs. 2–5 all execute closed loops when the hydrogen concentration is cycled. Additionally, when the concentration is varied over a limited range, the physical properties move back and forth between the absorption and desorption branches. Considering the large single-phase range in absorption ($2.1 \leqslant x \leqslant 2.8$), this is quite remarkable. For example, when starting to unload hydrogen near $x=2.4$ the system joins the desorption branch near $x=2.25$ (open circles in Figs. 3–5). This implies a disproportionation reaction, as in desorption at $x=2.25$ two phases coexist: (i) a high concentration hcp phase ($x\approx 2.7$), and (ii) a low concentration fcc phase ($x\approx 2.0$). But then the hydrogen has rearranged in such a way that the hydrogen concentration in regions which remain in the hexagonal phase has increased from $x=2.4$ (this was the case for the entire sample before starting desorption) to $x\approx 2.7$, a transformation which is obviously driven by the precipitation of the low concentration fcc phase.

The hysteresis described in the present work is considerably larger than what has been reported in literature for other $MH_x$ system. To our knowledge the only report of such large hysteresis is in thin film electroprecipitated nickel hydroxide ($NiO_2H_x$) electrodes[49] when the hydrogen concentration is varied between $x=1$ and 2. The major difference between bulk material and thin films lies in the fact that bulk material is able to expand in all three directions. Clamping of the film to the substrate on which it is deposited, induces a strong anisotropy in the expansion.[50] However, we also observed the phenomena mentioned in this paper in $YH_x$ films deposited on different, flexible (polymer) substrates. This implies that clamping is not responsible for the large hysteresis observed in $YH_x$. Further evidence is also provided by the absence of significant differences in lattice parameters of thin films and bulk material (compare Tables I and II).

Although it is not clear what microscopic mechanism is responsible for the hysteresis, it is reasonable to assume that it is related to large strains (and consequently stress) at the interface between fcc $YH_{1.9}$ and hcp $YH_{x\geqslant 2.1}$. $YH_x$ films are composed of small crystal grains with an average diameter smaller than 70 nm in the case of our 300-nm film.[51] Upon absorption of only a small quantity of hydrogen certain grains transform from a cubic structure to a hexagonal structure. As a result of the elastic interaction between neighboring crystallites, the entire film is transformed into the hcp phase at concentrations as low as $x=2.1$ (see Figs. 5 and 6). Apparently, the absence of such interaction during desorption allows individual crystallites to transform back to the fcc phase, while other crystallites remain in the (considerably more expanded) hcp phase. The absence of significant differences in electrochemical hydrogen loading and unloading of $LaH_x$ films,[52] which remain in the fcc phase for all $x\geqslant 2$, also supports our assumption that the hysteresis phenomena described in this paper are related to the structural fcc-hcp phase transition in the $YH_x$ system for $x>2$.

Owing to the stress-induced interaction the absorption isotherm is significantly different from the desorption isotherm. From Fig. 3 we can estimate the difference $\delta\Delta H_f$ in formation enthalpies associated with the fcc$\rightarrow$hcp and hcp$\rightarrow$fcc transitions. In desorption, the pressure plateau yields $\Delta H_f^{\gamma\rightarrow\beta}=-44.8$ kJ/mol H. As mentioned above during absorption the phase transition occurs within a narrow concentration range ($1.9\leqslant x\leqslant 2.1$) in which no plateau is observed. From the pressure at $x=2.0$ ($p_{H_2}=2.91\times 10^{-8}$ bar) we estimate $\Delta H_f^{\beta\rightarrow\gamma}=-40.3$ kJ/mol H. The difference $\delta\Delta H_f=4.5$ kJ/mol H is of the same order of magnitude as the values $\delta\Delta H_f=4.82$ and 8.88 kJ/mol H calculated from the hysteresis in the equilibrium potential for hydrogen intercalation in $NiO_2H_x$ (0.050 and 0.092 V for electrodes with and without cobalt hydroxide, respectively) in the work of Ta and Newman.[49] Considering that at every hydrogen concentration the $YH_x$ film can be in two different crystallographic states, it is interesting to compare our experimental value for $\delta\Delta H_f$ with the heat of transformation associated to similar structural transitions of pure yttrium and lanthanum. At elevated temperatures the heat involved in transforming hcp Y to bcc Y ($T_{tr}=1478\,^{\circ}C$) is $\Delta H_{tr}=4.99$ kJ/mol Y, while for the transition of double hcp La to fcc La ($T_{tr}=310\,^{\circ}C$) and of fcc La to bcc La ($T_{tr}=865\,^{\circ}C$) the heats of transformation amount to $\Delta H_{tr}=0.36$ and 3.12 kJ/mol La, respectively.[53] The fact that these values are of the same order of magnitude indicates that the difference we observe in our absorption and desorption isotherms may also be related to differences in the crystallographic configuration.

Finally, the importance of stress in the $YH_x$ thin films also follows from a comparison between x-ray spectra of as-deposited hcp-Y films and hydrogenated hcp $YH_3$ films. As mentioned in Sec. I, our as-deposited films are polycrystalline with a preferred orientation with the [002] direction perpendicular to the substrate surface. However, expansion upon hydrogenation of grains with the [002] direction parallel to the substrate will be hindered by neighboring material. The stress which is built up leads to plastic deformation and a reorientation of the crystal grains in such a way that the [002] directions of the different crystals align perpendicular to the substrate. This is expressed in x-ray measurements by a marked increase of the ratio of the (002) and (101) peak intensities upon hydrogenation of hcp Y ($I_{Y(002)}/I_{Y(101)}\approx 1.9$) to hcp $YH_3$ ($I_{YH_3(002)}/I_{YH_3(101)}\approx 20$). Furthermore, stress-induced deflection measurements[54,55] on $YH_x$ films show a compressive stress in the range 0.2–1.0 GPa (Refs. 55 and 56) upon hydrogenation of $YH_2$ to $YH_3$, which is at least an order of magnitude lower than what is expected on the basis of the 10% expansion along the hcp [002] direction. This can only be accounted for by a reorientation of the crystallites with the direction of maximum expansion perpendicular to the substrate.

## V. CONCLUSION

We have studied the hysteresis in the physical properties of thin $YH_x$ films in the reversible concentration range between fcc $YH_{2+\delta}$ and hcp $YH_{3-\delta}$. The differences between hydrogen absorption and desorption are considerably larger than what has been described previously in literature for any metal-hydrogen system. During desorption the crystallographic structure determined from *in situ* x-ray-diffraction experiments and the electrochemically measured pressure-composition isotherms indicate a large concentration range where the dihydride and trihydride phases coexist, identical to what has been found previously with bulk material. The optical transmittance exhibits an exponential decrease over the entire spectral range upon hydrogen unloading. The concentration dependency of both the transmittance and the electrical resistivity can be described by a simple model in which both columnar and layered distributions of the two coexisting phases is taken into account.

Upon hydrogen absorption a rapid structural fcc-hcp transition is observed at low concentrations ($1.9\leqslant x\leqslant 2.1$), which is accompanied by a decline of the characteristic dihydride transmittance window. A plateau in the pressure-composition isotherm was not found. Very remarkable is that at hydrogen concentrations above $x=2.1$ the film remains in the hcp phase and does not show any further expansion toward $x=3$. In this sense $YH_x$ is similar to $LaH_x$, which remains in the cubic structure at all concentrations $2\leqslant x\leqslant 3$, but exhibits a similar metal-insulator transition. The optical and electrical properties accompanying this metal-insulator transition can be interpreted in terms of hydrogen vacancies in stoichiometric $YH_3$. Removal of hydrogen vacancies leads to a reduction of charge carriers, and thus to a higher resistivity. The reduction in the density of defect states results in a lower optical absorbance and consequently a higher transmittance, in agreement with experimental results.

Finally, the extremely large hysteresis effects in the various physical properties are discussed in terms of strains (and consequently stress) at the interface between fcc $YH_2$ and hcp $YH_3$. On the basis of experiments on more flexible substrates and a comparison between bulk and thin-film lattice constants, we argue that the stress is not related to clamping of the film to the substrate. The stress between the two

phases results in a reorientation of the crystal grains within the film with the (002) direction perpendicular to the substrate.

## ACKNOWLEDGMENTS

We thank S. J. van der Molen, M. Kremers, and J. W. J. Kerssemakers from the Vrije Universiteit, P. A. Duine and P. van der Sluis (Philips Research Laboratory), and A. Pundt (University of Göttingen) for helpful discussions. This work is part of the research program of the Stichting voor Fundamenteel Onderzoek der Materie (FOM), financially supported by the Nederlandse Organisatie voor Wetenschappelijk Onderzoek (NWO) and Philips Research, and of the TMR Research Network ''Metal-hydride films with switchable physical properties.''

[1] *Hydrogen in Metals I and II, Topics in Applied Physics*, Vols. 28 and 29, edited by G. Alefeld and J. Völkl (Springer-Verlag, Berlin, 1978).

[2] *The Metal-Hydrogen System, Springer Series in Materials Science*, Vol. 21, edited by Y. Fukai (Springer-Verlag, Berlin, 1993).

[3] J.H. Weaver and C.G. Olson, Phys. Rev. B **16**, 731 (1977).

[4] J.H. Weaver, R. Rosei, and D.T. Peterson, Phys. Rev. B **19**, 4855 (1979).

[5] R. Feenstra, G.J. de Bruin-Hordijk, H.L.M. Bakker, R. Griessen, and D.G. de Groot, J. Phys. F: Met. Phys. **13**, L13 (1983).

[6] M. Nicolas, L. Dumoulin, and J.P. Burger, J. Appl. Phys. **60**, 3125 (1986).

[7] J.N. Huiberts, R. Griessen, J.H. Rector, R.J. Wijngaarden, J.P. Dekker, D.G. de Groot, and N.J. Koeman, Nature (London) **380**, 231 (1996).

[8] R. Griessen, J.N. Huiberts, M. Kremers, A.T.M. van Gogh, N.J. Koeman, J.P. Dekker, and P.H.L. Notten, J. Alloys Compd. **253–254**, 44 (1997).

[9] P. van der Sluis, M. Ouwerkerk, and P.A. Duine, Appl. Phys. Lett. **70**, 3356 (1997).

[10] P. van der Sluis, Appl. Phys. Lett. **73**, 1826 (1998).

[11] K. von Rottkay, M. Rubin, and P.A. Duine, J. Appl. Phys. **85**, 408 (1999).

[12] K. von Rottkay, M. Rubin, F. Michalak, R. Armitage, T. Richardson, J. Slack, and P.A. Duine, Electrochim. Acta **44**, 3093 (1999).

[13] D.G. Nagengast, A.T.M. van Gogh, E.S. Kooij, B. Dam, and R. Griessen, Appl. Phys. Lett. **75**, 2050 (1999).

[14] M. Kremers, N.J. Koeman, R. Griessen, P.H.L. Notten, R. Tolboom, P.J. Kelly, and P.A. Duine, Phys. Rev. B **57**, 4943 (1998).

[15] M. Ouwerkerk, Solid State Ionics **113-115**, 431 (1998).

[16] P.H.L. Notten, M. Kremers, and R. Griessen, J. Electrochem. Soc. **143**, 3348 (1996).

[17] E.S. Kooij, A.T.M. van Gogh, and R. Griessen, J. Electrochem. Soc. **146**, 2990 (1999).

[18] P. van der Sluis, Electrochim. Acta **44**, 3063 (1999).

[19] J. Hayoz, S. Sarbach, Th. Pillo, E. Boschung, D. Naumović, P. Aebi, and L. Schlapbach, Phys. Rev. B **58**, R4270 (1998).

[20] J.N. Huiberts, J.H. Rector, R.J. Wijngaarden, S. Jetten, D. de Groot, B. Dam, N.J. Koeman, R. Griessen, B. Hjörvarsson, S. Olafsson, and Y.S. Cho, J. Alloys Compd. **239**, 158 (1996).

[21] L.J. van der Pauw, Philips Res. Rep. **13**, 1 (1958).

[22] K.H.J. Buschow, P.C.P. Bouten, and A.R. Miedema, Rep. Prog. Phys. **45**, 937 (1982).

[23] R. Griessen and T. Riesterer, in *Hydrogen in Intermetallic Compounds I*, Topics in Applied Physics, Vol. 63, edited by L. Schlapbach (Springer-Verlag, Berlin, 1988), pp. 219–284.

[24] H.E. Flotow, D.W. Osborne, K. Otto, and B.M. Abraham, J. Chem. Phys. **38**, 2620 (1963).

[25] L.N. Yannopoulos, R.K. Edwards, and P.G. Wahlbeck, J. Phys. Chem. **69**, 2510 (1965).

[26] A.T.M. van Gogh, E.S. Kooij, and R. Griessen, Phys. Rev. Lett. **83**, 4614 (1999).

[27] W.M. Mueller, J.P. Blackledge, and G.G. Libowitz, *Metal Hydrides* (Academic Press, New York, 1968).

[28] P. Vajda, in *Handbook on the Physics and Chemistry of Rare Earths*, edited by K.A. Gschneider, Jr. and L. Eyring (Elsevier, Amsterdam, 1995), Vol. 20, pp. 207–291.

[29] T.J. Udovic, Q. Huang, and J.J. Rush, J. Phys. Chem. Solids **57**, 423 (1996).

[30] A. Remhof, G. Song, Ch. Sutter, A. Schreyer, R. Siebrecht, H. Zabel, F. Güthoff, and J. Windgasse, Phys. Rev. B **59**, 6689 (1999).

[31] F.H. Spedding and B.J. Beaudry, J. Less-Common Met. **25**, 61 (1971).

[32] K. Dialer and B. Frank, Z. Naturforsch. B **15**, 58 (1960).

[33] A. Pebler and W.E. Wallace, J. Phys. Chem. **66**, 148 (1962).

[34] C.E. Lundin and J.P. Blackledge, J. Electrochem. Soc. **109**, 838 (1962).

[35] H.E. Flotow, D.W. Osborne, and K. Otto, J. Chem. Phys. **36**, 866 (1962).

[36] M. Born and E. Wolf, *Principles of Optics*, 6th ed. (Cambridge University Press, Cambridge, 1980).

[37] We assume that the optical properties of the palladium cap layer are constant. In fact, $PdH_{0.7}$ has a higher transmittance than pure palladium (Refs. 11 and 12), but the plateau pressure of the $PdH_x$ system at room temperature is approximately $10^{-2}$ bar (Ref. 27). From Fig. 3 (open squares) we can conclude that this implies a low hydrogen concentration within the palladium over the entire concentration range studied here ($2.0 \leqslant x \leqslant 2.7$).

[38] S.N. Sun, Y. Wang, and M.Y. Chou, Phys. Rev. B **49**, 6481 (1994).

[39] N.F. Mott, *Metal-Insulator Transitions*, 2nd ed. (Taylor & Francis, Bristol, 1990).

[40] A. Husmann, D.S. Jin, Y.V. Zastavker, T.F. Rosenbaum, X. Yao, and J.M. Honig, Science **274**, 1874 (1996).

[41] *Metal-Insulator Transitions Revisited*, edited by P.P. Edwards and C.N.R. Rao (Taylor & Francis, Bristol, 1995).

[42] S.J. van der Molen, D.G. Nagengast, A.T.M. van Gogh, J. Kalkman, and R. Griessen (unpublished).

[43] P. Vajda and J.N. Daou, Phys. Rev. Lett. **66**, 3176 (1991).

[44] J.N. Daou and P. Vajda, Phys. Rev. B **45**, 10 907 (1992).

[45] K.K. Ng, F.C. Zhang, V.I. Anisimov, and T.M. Rice, Phys. Rev. Lett. **78**, 1311 (1997).

[46] K.K. Ng, F.C. Zhang, V.I. Anisimov, and T.M. Rice, Phys. Rev. B **59**, 5398 (1999).

[47] J.R. Lacher, Proc. R. Soc. London, Ser. A **161**, 525 (1937).
[48] R. Feenstra, R. Griessen, and D.G. de Groot, J. Phys. F: Met. Phys. **16**, 1933 (1986).
[49] K.P. Ta and J. Newman, J. Electrochem. Soc. **146**, 2769 (1999).
[50] G. Song, A. Remhof, K. Theis-Bröhl, and H. Zabel, Phys. Rev. Lett. **79**, 5062 (1997).
[51] S.J. van der Molen, J.W.J. Kerssemakers, J.H. Rector, N.J. Koeman, B. Dam, and R. Griessen, J. Appl. Phys. **86**, 6107 (1999).
[52] E.S. Kooij and J. Isidorsson (unpublished).
[53] *CRC Handbook of Chemistry and Physics*, 77th ed., edited by D.R. Lide (CRC Press, Boca Raton, FL, 1996).
[54] M. Bicker, U. von Hülsen, U. Laudahn, A. Pundt, and U. Geyer, Rev. Sci. Instrum. **69**, 460 (1998).
[55] J.W.J. Kerssemakers (private communication).
[56] M. Dornheim, S.J. van der Molen, E.S. Kooij, J.W.J. Kerssemakers, and A. Pundt (unpublished).